A Local Hybrid Exchange Functional Approximation from First Principles

Christof Holzer[1, a)] and Yannick J. Franzke[2, a)]

[1)]*Institute of Theoretical Solid State Physics, Karlsruhe Institute of Technology (KIT), Wolfgang-Gaede-Straße 1, 76131 Karlsruhe, Germany*

[2)]*Fachbereich Chemie, Philipps–Universität Marburg, Hans-Meerwein-Straße 4, 35032 Marburg, Germany*

(*Email for correspondence: yannick.franzke@chemie.uni-marburg.de)

(*Email for correspondence: christof.holzer@kit.edu)

(Dated: 23 May 2022)

Local hybrid functionals are a more flexible class of density functional approximations allowing for a position-dependent admixture of exact exchange. This additional flexibility, however, comes with a more involved mathematical form and a more complicated design. A common denominator for previously constructed local hybrid funtionals is usage of thermochemical benchmark data to construct these functionals. Herein, we design a local hybrid functional without relying on benchmark data. Instead, we construct it in a more *ab initio* manner, following the principles of modern *meta*-generalized gradient approximations and considering theoretical constrains. To achieve this, we make use of the density matrix expansion and a local mixing function based on an approximate correlation length. The accuracy of the developed density functional approximation is assessed for thermochemistry, excitation energies, polarizabilities, magnetizabilities, NMR spin–spin coupling constants, NMR shieldings and shifts, as well as EPR *g*-tensors and hyperfine coupling constants. Here, the new exchange functional shows a robust performance and is especially well suited for atomization energies, barrier heights, excitation energies, NMR coupling constants, and EPR properties, whereas it looses some ground for the NMR shifts. Therefore, the designed functional is a major step forwards for functionals that have been designed from first principles.

[a)]C. Holzer and Y. J. Franzke contributed equally to this work.

I. INTRODUCTION

The incorporation of exact exchange or Hartree–Fock (HF) exchange into semilocal density functional theory (DFT) was a milestone in computational chemistry.[1–3] Today, DFT is probably the most widely applied computational method in chemistry and material science due to its favorable cost-accuracy ratio. Global hybrid functionals such as B3LYP,[4–6] PBE0,[7,8] or TPSSh [9,10] use a fixed or static amount of HF exchange. Typically, global hybrid functionals use 5–25% of HF exchange.[3] While this leads to accurate results for many chemical properties, such a rigid admixture of exact exchange is not suited for charge-transfer excitations or the dissociation curve. Global hybrid functionals with the given amount of exact exchange still feature a self-interaction error. This is especially pronounced in one-electron regions. Therefore, range-separated hybrid (RSH) functionals, which typically use a significantly larger amount of exact exchange in the long-range region, were introduced.[11–14]

Local hybrid functionals (LHFs) feature a position-dependent admixture of Hartree–Fock exchange via a local mixing function (LMF).[15] Thus, the LMF increases the flexibility of the functional as the amount of HF exchange can be increased or decreased in certain regions and LHFs are a more general class of hybrid density functional approximations. Compared to range-separated hybrid functionals, this functional form results in a smoother transition from spatial regions with a small amount of HF exchange to regions with a large amount of HF exchange, as it is possible to interpolate between the semilocal DFT and HF limits. However, LHFs introduce a gauge dependence of the exact-exchange energy density.[16] Thus, a so-called calibration function [16–18] (CF) is introduced in modern local hybrid functionals such as LH14t-calPBE [17] and LH20t.[19]

The LMF is the key ingredient of LHFs and different ansätze were suggested.[20,21] The first and still most prominent method to distinguish the electronic regions is the iso-orbital indicator (t-LMF).[15] This allows to identify one-electron regions, those accurate description requires an increased amount of exact exchange. Other approaches are based on the correlation length (z-LMF),[22] reduced (spin) density gradients (s-LMF),[23,24] the density overlap regions indicator (DORI-LMF),[25,26] or the second-order Görling–Levy perturbation limit [27] of the correlation (PSTS-LMF).[28] We have recently carried out benchmark calculations of electric and magnetic response properties for LHFs based on different LMFs.[29] This showed encouraging results for Johnson's LHF [22] based on the correlation length—especially for heavy elements. We note that this LMF is also advantageous in numerically demanding cases and results in a smooth convergence

behavior.[30] However, only one functional based on this LMF was optimized,[22] which consists of Becke's 1988 exchange [31] and correlation terms.[32] Moreover, this functional does not make use of a calibration function, which is commonly included in the latest generation of LHFs based on the iso-orbital indicator. Therefore, we will first re-parameterize this functional with the Becke 1995 correlation term [33] and also add a CF in this work.

In a second step, we will design a more sophisticated local hybrid functional from first principles. Modern (range-separated) hybrid and local hybrid functionals are typically optimized using (large) thermochemical test sets. While this may result in well performing density functionals approximations for the properties considered in the design, it may also come with a loss of generality and physical insight.[34,35] In contrast, modern semilocal functionals [36–39] are first designed to include (almost) all known theoretical constrains and then applied to large benchmark test sets. Herein, we will follow this route and adapt it to the form of local hybrid functionals.

In addition to electron correlation, an accurate description of the electronic structure throughout the periodic table of elements necessitates a proper treatment of relativistic effects.[40–46] Herein, we will also generalize the two-component framework for open-shell systems developed in Ref. 47 to include the z-LMF [22] and PSTS-LMF, [28] as well as higher-order derivatives to add the so-called calibration function of modern local hybrid functionals.[19,21] It is shown that these functionals lead to substantially improved results for EPR properties, which are a problematic case for the first and second generation of t-LMF based functionals.[47]

The paper is structured as follows. First, we will discuss the theoretical framework. In doing so, the optimization of a density functional approximation based on the correlation length from first principles is described. Then, the accuracy of the developed functionals is assessed for thermochemisty, excitations, polarizabilities, magnetizabilities, and NMR/EPR properties.

II. THEORY AND IMPLEMENTATION

We will first review local hybrid functionals within an unrestricted Kohn–Sham (UKS) formalism and the calibration function in subsections II A and II B. This ensures that all optimized parameters are described herein. Furthermore, the generalization to a two-component framework is described in Sec. II C. In subsection II D, we construct an optimized LHF based on the correlation length similar to Johnson's work.[22] Motivated by the success of this approach, a local hybrid exchange functional is constructed from first principles in subsection II E.

A. Unrestricted Kohn–Sham Formalism for LHFs

In an UKS framework, the exchange-correlation (XC) energy is given by

$$E_{\mathrm{XC}}^{\mathrm{LHF}} = \sum_{\sigma=\alpha,\beta} \int d\vec{r} \; \left[\{1 - a_\sigma(\vec{r})\} \, e_{\mathrm{X},\sigma}^{\mathrm{DFT}}(\vec{r}) + a_\sigma(\vec{r}) e_{\mathrm{X},\sigma}^{\mathrm{HF}}(\vec{r}) \right] + E_{\mathrm{C}}^{\mathrm{DFT}}(\vec{r}), \tag{1}$$

where a is the LMF, $e_{\mathrm{X},\sigma}^{\mathrm{DFT}}$ is the semilocal DFT exchange energy density, and $e_{\mathrm{X},\sigma}^{\mathrm{HF}}$ denotes the exact-exchange or Hartree–Fock exchange energy density. $E_{\mathrm{C}}^{\mathrm{DFT}}$ refers to the correlation energy. The LMF may depend on the spin quantities or total quantities. LMFs based on the latter include spin polarization and are called common LMFs.[48] To carry out the integration in Eq. 1, Plessow and Weigend suggested to use a seminumerical scheme,[49] as this also computes the LMF, the exact-exchange energy contribution, and the semilocal DFT exchange energy density on a grid. The exact-exchange term follows as

$$e_{\mathrm{X},\sigma}^{\mathrm{HF}}(\vec{r}) = -\frac{1}{2} \sum_{pqrs} D_{pq}^{\sigma} D_{rs}^{\sigma} \int d\vec{r}\,' \frac{\phi_p^*(\vec{r}) \phi_r(\vec{r}) \phi_q^*(\vec{r}\,') \phi_s(\vec{r}\,')}{|\vec{r} - \vec{r}\,'|}, \tag{2}$$

where the integration with respect to $\vec{r}\,'$ is evaluated. ϕ_p and D_{pq}^{σ} denote the one-electron basis functions and the spin density matrix, respectively. The remaining integration with respect to $\vec{r}$ is performed numerically on a grid. Therefore, the position-dependent admixture of exact exchange is directly included in the DFT routines according to

$$E_{\mathrm{X}}^{\mathrm{LHF}} = \sum_{\sigma} \sum_{g} w_g \left[1 - a_\sigma(\vec{r}_g) \right] \, e_{\mathrm{X},\sigma}^{\mathrm{HF}}(\vec{r}_g), \tag{3}$$

with g denoting a grid point. This LHF scheme was later applied self-consistently [50] to various molecular properties such as geometry gradients,[29,51] excitation energies and polarizabilities,[52–55] ionization potentials with the *GW* method,[29,56] magnetizabilities,[29] and nuclear magnetic resonance (NMR) parameters.[29,30,57–60] The latter were also used to compute the magnetically induced current density and ring current strengths of aromatic systems.[29] The reworked implementations of these properties are described in Refs. 29 and 55.

First, the LMF may be formulated based on the iso-orbital indicator.[15] The respective t-LMF reads

$$a_\sigma(\vec{r}) = c_t \frac{\tau_\sigma^{\mathrm{vW}}}{\tau_\sigma} = c_t \frac{|\nabla \rho_\sigma|^2}{8 \rho_\sigma \tau_\sigma}. \tag{4}$$

Here, the kinetic-energy density τ is compared to the von Weizsäcker approximation τ^{vW}.[61] ρ_σ denotes the (spin) density. In case of a common LMF, the total (kinetic-energy) densities are used. The prefactor c_t in Eq. 4 is an optimized parameter.

Second, Johnson introduced a LMF using the correlation length z according to[22]

$$a_\sigma(\vec{r}) = \mathrm{erf}(c_z\, z_{\sigma\sigma}) \tag{5}$$

with the empirical parameter c_z. Note that only the contribution of parallel spins is considered. Here, the correlation length is computed with the exchange potential U_X and the exchange hole h_X as

$$z_{\sigma\sigma'} = c_{\sigma\sigma'}\left(|U_{\mathrm{X},\sigma}|^{-1} + |U_{\mathrm{X},\sigma'}|^{-1}\right), \tag{6}$$

$$U_{\mathrm{X},\sigma} = \int ds\, \frac{1}{s}|h_{\mathrm{X},\sigma}(\vec{r},s)|, \tag{7}$$

where $c_{\sigma\sigma'}$ are given by $c_{\alpha\beta} = 0.63$ and $c_{\sigma\sigma} = 0.88$.[32] Notably, this z-LMF depends explicitly on the underlying exchange functional.

B. Calibration Function

Tao *et al.* pointed out that the exchange-energy densities are gauge dependent.[16] This ambiguity leads to the so-called gauge problem.[16,17,62,63] The respective gauge transformation reads

$$e_{\mathrm{X},\sigma}^{\mathrm{HF,DFT}}(\vec{r}) = e_{\mathrm{X},\sigma}^{\mathrm{HF,DFT}}(\vec{r}) + \Lambda_\sigma(\vec{r}). \tag{8}$$

This gauge transformation term or calibration function $\Lambda_\sigma(\vec{r})$ is required to meet the condition

$$\int d\vec{r}\, \Lambda_\sigma(\vec{r}) = 0. \tag{9}$$

Hence, this does not change the exchange energy of a global hybrid functional. However, the term including the LMF, $\int d\vec{r}\, [1 - a_\sigma(\vec{r})]\Lambda_\sigma(\vec{r})$, is not zero. Including the calibration function $\Lambda_\sigma(\vec{r})$ in a LHF leads to the correlation-exchange energy expression

$$E_\mathrm{XC}^\mathrm{LHF} = \sum_\sigma \int d\vec{r}\left[(1 - a_\sigma(\vec{r}))\left\{e_{\mathrm{X},\sigma}^\mathrm{DFT}(\vec{r}) + \Lambda_\sigma(\vec{r})\right\} + a_\sigma(\vec{r}) e_{\mathrm{X},\sigma}^\mathrm{HF}(\vec{r})\right] + E_\mathrm{C}^\mathrm{DFT}(\vec{r}). \tag{10}$$

Different CFs were suggested in the literature.[16–18] In the original ansatz by Tao *et al.*, a CF based on the exact-exchange energy density, its first and second derivatives is constructed.[16] Such a CF is numerically demanding and consequently Kaupp *et al.* derived CFs based on the electron density and its derivatives up to terms depending on $\vec{\nabla}\tau$.[17,18] Herein, we use the so-called pig2 (second-order partial integration gauge) calibration function. This CF reads [18]

$$\begin{aligned}\Lambda_\sigma(\vec{r}) = \quad & f_1 f_2\, \rho_\sigma^{4/3}\, s_\sigma^2 \cdot \frac{\mathrm{d}^2 F_d(s_\sigma)}{\mathrm{d}s_\sigma^2} \cdot \left(p_\sigma - \frac{4}{3}s_\sigma^2\right), \\ & + f_1 f_2\, \rho_\sigma^{4/3}\, s_\sigma \cdot \frac{\mathrm{d}F_d(s_\sigma)}{\mathrm{d}s_\sigma} \cdot \left(p_\sigma + q_\sigma - \frac{5}{3}s_\sigma^2\right),\end{aligned} \tag{11}$$

where f_1 and f_2 are empirical prefactors, while s_σ, q_σ, and p_σ are the reduced (spin) density gradient, the reduced density Laplacian, and the reduced density Hessian, respectively. F_d is a cut-off or damping function, which is typically computed based on Becke's 1988 [31] or 1998 exchange functional.[64] The reduced spin density gradient s_σ is defined as

$$s_\sigma = \frac{1}{k}\frac{\gamma_{\sigma\sigma}^{1/2}}{\rho_\sigma^{4/3}}, \tag{12}$$

$$k = 2(6\pi^2)^{1/3}, \tag{13}$$

$$\gamma_{\sigma\zeta} = \vec{\nabla}^{\mathrm{T}}\rho_\sigma \cdot \vec{\nabla}\rho_\zeta, \tag{14}$$

and the remaining density-dependent quantities q_σ and p_σ are given as

$$q_\sigma = \frac{1}{k^2}\frac{\vec{\nabla}^{\mathrm{T}}\vec{\nabla}\rho_\sigma}{\rho_\sigma^{5/3}}, \tag{15}$$

$$p_\sigma = \frac{1}{k^2}\frac{\eta_{\sigma,\sigma\sigma}}{\gamma_{\sigma\sigma}\cdot\rho_\sigma^{5/3}}, \tag{16}$$

$$\eta_{\theta,\sigma\zeta} = \vec{\nabla}^{\mathrm{T}}\rho_\sigma \cdot \vec{\nabla}\vec{\nabla}^{\mathrm{T}}\rho_\theta \cdot \vec{\nabla}\rho_\zeta. \tag{17}$$

We use a damping function of the Becke 1988 exchange functional [31] given as

$$F_d(s_\sigma) = \frac{k^2\beta}{1 + 6\beta k \cdot s_\sigma \cdot \mathrm{asinh}(k \cdot s_\sigma)} \tag{18}$$

with an empirical parameter β. Note that this CF is already implemented for non-relativistic or scalar-relativistic one-component approaches up to second-order properties.[18,58,60] However, this CF also increases the numerical demands and comparably large integration grids may be needed.[17,29,30] Also, the thresholds for the XC integration need to be tightened for the SCF and response equations to ensure a smoother convergence.[30]

C. Generalization to a Non-Collinear Two-Component Framework

A self-consistent treatment of spin-orbit coupling necessitates a generalized two-component Kohn–Sham formalism. This requires not only the spin excess density but the complete spin magnetization vector, which is is introduced according to

$$\vec{m} = \sum_i \varphi_i^\dagger \vec{\sigma} \varphi_i \tag{19}$$

with the two-component spinor function φ_i and the vector $\vec{\sigma}$ containing the (2 × 2) Pauli spin matrices. The total electron density ρ and the non-collinear spin density ρ_s are given as [65,66]

$$\rho = \sum_i \varphi_i^\dagger \varphi_i, \tag{20}$$

$$\rho_s = (\vec{m} \cdot \vec{m})^{1/2}. \tag{21}$$

In a basis set representation, the non-collinear exchange-correlation energy depends on the total density matrix $\mathbf{M}_0$ and the three spin vector density matrices $\mathbf{M}_i$ with $i = x, y, z$. These are defined as [65,66]

$$\mathbf{M}_0 = \mathrm{Re}(\mathbf{P}^{\alpha\alpha}) + \mathrm{Re}(\mathbf{P}^{\beta\beta}), \tag{22}$$

$$\mathbf{M}_x = \mathrm{Re}(\mathbf{P}^{\alpha\beta}) + \mathrm{Re}(\mathbf{P}^{\beta\alpha}), \tag{23}$$

$$\mathbf{M}_y = \mathrm{Im}(\mathbf{P}^{\alpha\beta}) - \mathrm{Im}(\mathbf{P}^{\beta\alpha}), \tag{24}$$

$$\mathbf{M}_z = \mathrm{Re}(\mathbf{P}^{\alpha\alpha}) - \mathrm{Re}(\mathbf{P}^{\beta\beta}). \tag{25}$$

The XC potential follows as

$$\mathbf{V}_{\mathrm{XC}}[M_0(\vec{r}), M_i(\vec{r})] = \frac{\delta E_{\mathrm{XC}}[M_0(\vec{r}), \rho_i(\vec{r})]}{\delta M_0(\vec{r})} + \sum_{i=x,y,z} \vec{\sigma}_i \frac{\delta E_{\mathrm{XC}}[M_0(\vec{r}), M_i(\vec{r})]}{\delta M_i(\vec{r})}. \tag{26}$$

The generalization of a non-relativistic spin-density functional is done using the spin-up and spin-down densities [67,68]

$$\rho^\uparrow = (\rho + \rho_s)/2, \tag{27}$$

$$\rho^\downarrow = (\rho - \rho_s)/2. \tag{28}$$

Only considering $\mathbf{M}_0$ and $\mathbf{M}_z$ results in the UKS limit. Therefore, an unrestricted Kohn–Sham implementation of the XC potential and the XC energy can be extended straightforwardly.[67] This involves the following major steps. First, the electron (spin) density and its derivatives such as the gradient and the Laplacian or the kinetic-energy density are evaluated at a given grid point. Second, the respective derivatives are multiplied with its spin density matrix contribution and the sum of all three vector components is formed. The inverse of the total spin density is used as a prefactor. Third, the spin-up and spin-down contributions are constructed. Then, the exchange and correlation functional expressions can be evaluated similar to UKS. For further details, we refer to Refs. 67 and 69. Herein, we have implemented this scheme up to the Hessian of the electron density and the gradient of the kinetic-energy density to evaluate all calibration functions

described in Ref. 18. A generalization of spin-dependent local mixing function is more involved and many modern LHFs based on the t-LMF use a common local mixing function. Therefore, the implementation of the 2c t-LMF is still restricted to the common variant. Thus, LH07t-SVWN [70] or LH14t-calPBE [17] are not yet available. Moreover, current-dependent terms arise as spin–orbit coupling is closely related to magnetic induction and these are neglected herein,[71] however, their implementation will be presented elsewhere.

D. Optimized Functionals based on the Correlation Length

The original LHF of Johnson, termed LHJ14 herein, is based on Becke's 1988 (B88) exchange contribution [31] and his 1988 modified correlation term.[32] The latter is rarely used in common hybrid and range-separated hybrid density functional approximations. Thus, we use Becke's 1995 (B95) correlation term [33] instead and re-optimized the parameter c_z in Eq. 5. Furthermore, a pig2 calibration function including the damping function of the B88 exchange contribution was added. The parameters for the calibration function were taken from Ref. 18 for the B88 functional.[31] The parameter c_z, controlling the mixing of exact exchange and local exchange, was subsequently fitted to the exchange-correlation energies of the rare-gas atoms He to Xe. For the fitting procedure, the sum of exchange and correlation energies were fitted to allow for error cancellation of the LHF exchange together with the B95 correlation functional.[33] The obtained parameters are summarized in Tab. I. An optimized parameter $c_z = 0.20$ is obtained.

LHJ-HF is a good example of outlining the simplicity at which sophisticated, calibrated LHFs can be obtained. Only data available from atomic calculations enter each component, making it strictly independent from any thermochemical data, frequently used to parametrize density functional approximations. Yet, more elaborate functionals may be needed to fully exploit the possibilities of the local mixing of exact exchange. In the next section, we will therefore outline a more

TABLE I. Parameters found for LHJ-HFcal. The simplified version LHJ-HF does not consider the parameters of the pig2 calibration function (f_1, f_2) and the Becke damping function (β). Parameters were fitted to the exchange-correlation energies of the rare-gas atoms He to Xe.

c_z	f_1	f_2	β
0.20	−2.244	0.821	0.003667

rigorous approach, which will distinguish between diverse spatial regions in the density.

E. Designing a Local Hybrid Exchange Functional from First Principles

A common denominator for previously constructed local hybrid funtionals is usage of thermochemical benchmark data to construct these functionals. In this paper, we aim at constructing a local hybrid exchange functional without relying on benchmark data. Instead, we construct it in a more *ab initio* manner, following the principles of previous metaGGA functionals.[9,36,37]

We define the local exchange part e_{X} as usual using an enhancement factor F_{X},

$$E_{\mathrm{X}} = \sum_{\sigma=\alpha,\beta} \int d\vec{r}\, F_{\mathrm{X}}(\rho_\sigma, \boldsymbol{\nabla}\rho_\sigma, \tau_\sigma; \vec{r}) \cdot e_{\mathrm{X}}^{\mathrm{unif}}(\rho_\sigma; \vec{r}), \tag{29}$$

where the exchange energy density from the local (spin) density approximation is defined as

$$e_{\mathrm{X}}^{\mathrm{LSDA}}(\rho_\sigma; \vec{r}) = \rho_\sigma e_{\mathrm{X}}^{\mathrm{unif}}(\rho_\sigma; \vec{r}) = -\frac{3\rho_\sigma}{4\pi}(3\pi^2\rho_\sigma)^{1/3}. \tag{30}$$

As in many recent density functional approximations (DFAs), we chose a semilocal enhancement factor, where F_{X} is a function of the density ρ_σ, the gradient of the density $\boldsymbol{\nabla}\rho_\sigma$, and the kinetic energy density τ_σ. As the exchange enhancement factor only depends on a single spin coordinate, it is dropped in the following equations. Particularly, we adopt the density matrix expansion (DME) approach of Tao and Mo,[36] which has been shown to perform well for solids.[72–74] Within the DME of Tao and Mo, the enhancement factor $F_{\mathrm{X}}^{\mathrm{DME}}$ is given as

$$F_{\mathrm{X}}^{\mathrm{DME}} = \frac{1}{f_{\mathrm{X}}^2} + \frac{7R_{\mathrm{X}}}{9f_{\mathrm{X}}^4}. \tag{31}$$

The auxiliary quantities R_{X} and f_{X} are defined as

$$R_{\mathrm{X}} = 1 + \frac{594}{54}y - \left[\tau - 3(\lambda_{\mathrm{X}}^2 - \lambda_{\mathrm{X}} + 0.5) \times \left(\tau - \tau^{\mathrm{unif}} - \frac{|\nabla\rho|^2}{72\rho}\right)\right] \frac{1}{\tau^{\mathrm{unif}}} \tag{32}$$

and

$$f_{\mathrm{X}} = \left[1 + 10\frac{70y}{27} + \beta_{\mathrm{X}} y^2\right] \tag{33}$$

with $\tau^{\mathrm{unif}} = (3/10)(3\pi^2)^{2/3}\rho^{5/3}$. λ is a real number between 0.5 and 1, describing the coordinate transformation. $\lambda = 1$ corresponds to the conventional exchange hole.[36] Furthermore, $y = (2\lambda - 1)^2 p$, is a scaled version of the reduced density gradient depending on the coordinate transformation with $p = s^2$. For a local hybrid functional, exact and local exchange are combined.

Therefore, we choose $\lambda_X = 1$, corresponding to the untransformed exchange hole. The parameter β_X will be determined later. As outlined by Tao and Mo, the DME is not exact for slowly varying densities. Hence, it is advisable to pair it with a fourth-order gradient correction.[36] We use the same expressions as Tao and Mo for the correction in the slowly varying limit

$$\begin{aligned} F_X^{SC} = &\{1 + 10[(10/81 + 50p/729)p + 146\tilde{q}^2/2025 \\ &- (73\tilde{q}/405)\,[3\tau^{vW}/(5\tau)](1 - \tau^{vW}/\tau)]\}^{1/10} \end{aligned} \tag{34}$$

with $\tilde{q} = (9/20)(\alpha - 1) + 2p/3$, and $\alpha = \left(\tau - \tau^{vW}\right)/\tau^{unif}$.[36] The interpolation between F_X^{DME} and F_X^{SC} is also unaltered from the Tao–Mo functional, yielding the final enhancement factor F_X as

$$F_X = wF_X^{DME} + (1 - w)F_X^{SC} \tag{35}$$

with the interpolation function $w = [(\tau^{vW}/\tau)^2 + 3(\tau^{vW}/\tau)^3]/[1 + (\tau^{vW}/\tau)^3]^2$. As missing piece to construct a local hybrid functional, a suitable mixing function, augmenting the DME with exact exchange, is needed. We adopt an approach similar to the correlation length as suggested by Johnson.[22] Using an approximated correlation length z^{DME},

$$z_{\sigma\sigma'}^{DME} = (|U_\sigma|^{-1} + |U_{\sigma'}|^{-1}), \tag{36}$$

we define U as

$$U_\sigma = c_F[(1 + \zeta)\rho_\sigma]^{1/3}\left(\frac{1}{f_L^2} + \frac{7R_L}{9f_L^4}\right) \tag{37}$$

with $c_F = 3/8 \cdot 4^{2/3}(3/\pi)^{1/3}$ and $\zeta = (\rho_\sigma - \rho_{\sigma'})/(\rho_\sigma + \rho_{\sigma'})$. $U_{\sigma'}$ is obtained by reversing the spin indices. The expressions of R_L and f_L are equivalent to those in the equations 32 and 33. The different subscripts hint at the parameters β_L and λ_L being different from those used in Eqs. 32 and 33. To map $z_{\sigma\sigma'}^{DME}$ to the interval $\{0, 1\}$, we define the local mixing function a^{DME} as

$$a^{DME} = 1 - \exp\left(-c_L \cdot z_{\sigma\sigma'}^{DME}\right). \tag{38}$$

The parameters $\beta_L = 79.873$ and $\lambda_L = 0.6866$ are set to the values obtained for the hydrogen atom by Tao and Mo.[36] Therefore, the correlation length is measured for the transformed exchange hole. Contrary, for the exchange enhancement factor in Eq. 31, a value of $\lambda_X = 1.0$ is set, parametrizing the untransformed exchange hole.

What is left to be determined are only the parameters β_X from the DME, parameterizing the untransformed exchange hole, and c_L, accounting for the inclusion of exact exchange through the LMF. The latter two parameters are obtained by fitting them to spin-unpolarized two-electron

TABLE II. Parameters of TMHF. c_L, β_L, and λ_L are employed for the LMF, while β_X and λ_X are used for the exchange density. Note that all parameters were derived from physical constraints

c_L	β_L	λ_L	β_X	λ_X
0.18	79.873	0.6866	265.25	1.0

densities.[75,76] As our aim is to design a functional without any prior exact knowledge of total exchange-correlation energies, even atomic ones, we fit the parameters to theoretical considerations. First, in the low density limit, which challenges the Lieb–Oxford bound more, the energy is constrained by $e_X = 1.174\, e_X^{LSDA}$.[76] Second, in the high density limit, we expect the results to be closer to the Hartree–Fock solution, i.e. $e_X = 1.16588\, e_X^{LSDA}$.[77] Both of these values can be derived analytically. To guide the optimization, we choose two two-electron systems, as for those Hartree-Fock exchange provides solutions close to the exact solution.[75] For the low-density limit, He is used, while we chose Hg^{78+} as guide for the high-density limit. For both atoms, we evaluate the corresponding LSDA exchange energies at the Hartree-Fock solution using saturated basis sets. For He and Hg^{78+}, we find LSDA energies of -0.885 and -42.699 Hartree. Both of these values are within 2 mHartree of those obtained for the exact density.[75] Multiplying with the analytic prefactors yields -1.039 and -49.781 Hartree, respectively. Finally, we optimize β_X for a given value of c_L, yielding possible pairs of solutions. We chose the pair with the highest value for c_L, yielding $c_L = 0.18$ and $\beta_X = 265.25$. It shall be noted that while the Lieb–Oxford bound was taken into account during the evaluation of the parameters, the derived exchange approximation may still violate it for certain systems and basis sets, as it is not strictly constrained by it. Furthermore, our functional certainly violates the conjectured local version of the Lieb–Oxford bound. The latter issue could be remedied by a gauge transformation. For convenience, the parameters of the developed functional (TMHF) are summarized in Tab. II. We pair this local hybrid exchange functional again with the B95 correlation functional, as the latter has shown to work well in conjunction with local hybrid exchange functionals.[19]

The DME local mixing function is outlined in Fig. 1 for Li_2 at 5.0 bohrs and at 10.0 bohrs. It clearly shows the different behavior between bonded and stretched Li_2. In the former case, the LMF has a local minimum at the center, while in the latter case a local maximum is found. Comparably, at the bond center the amount of exact exchange included is raised by roughly 25% in the stretched dimer. This effect will lead to significantly improved barrier heights, while not

degrading the overall performance for other properties. In Ref. 78 it was noticed that, due to the order-of-limits problem of the interpolation function, stretched Li_2 will not converge with the Tao–Mo functional using the aug-cc-pVQZ basis set,[79–81] which was confirmed by us. The root of this issue is a singularity located at the center between the two Li atoms, caused by the order-of-limits problem.[78] TMHF, however, converges smoothly for the stretched Li_2. This can can be attributed to the large amount of exact exchange incorporated at the center of the stretched bond, and the increased numerical rigor of our implementation. Still, the local exchange part of TMHF is plagued by the order-of-limits problem, but for stretched bonds it is expected to be less harmful. Near the nucleus, where the LMF approaches 0, the singularity from the order-of-limits problem is, however, not countered. Therefore, no improvements of TMHF over the initial Tao–Mo functional (or other standard metaGGA functionals) are expected for properties that are sensitive to the exchange contribution and the electron density in the vicinity of the nuclei.

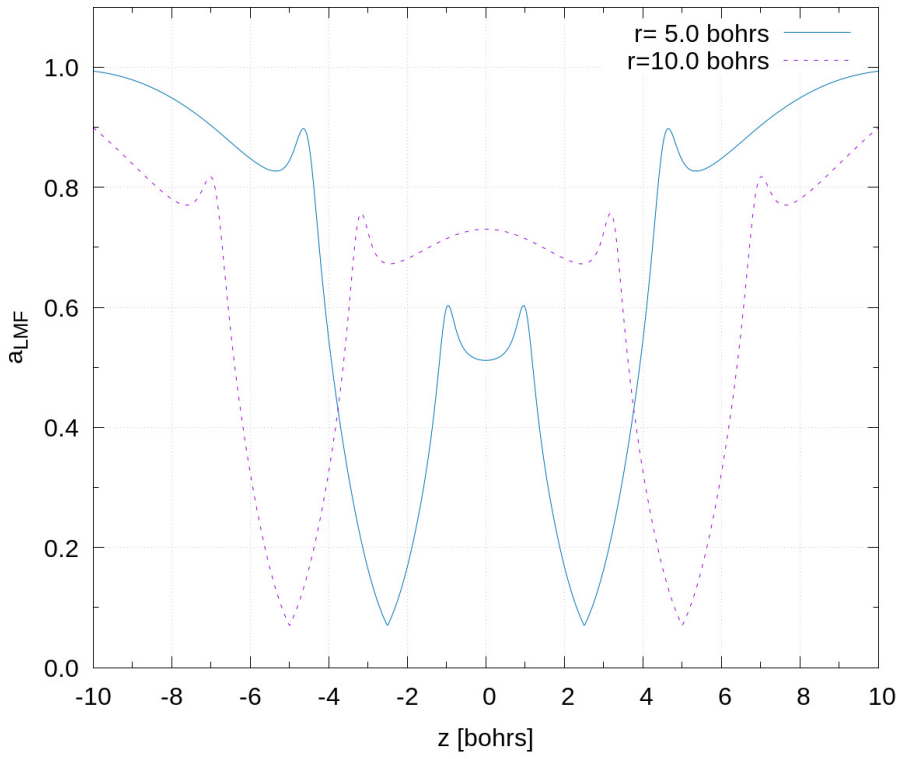

FIG. 1. DME local mixing function as a function of z at various distances between two Li atoms, calculated using the aug-cc-pVQZ basis set. Distance between the two Li atoms is $r = 5.0$ bohrs (solid line) and at $r = 10.0$ bohrs (dashed line).

F. Implementation

The outlined functionals were implemented into the TURBOMOLE program suite.[82–85] The mathematical functions for the LMFs were generated using MAPLE scripts,[86] while the individual exchange and correlation functional terms are computed with Libxc.[87–89] As stated in Ref. 47, for 2c calculations it is advantageous to work with "common" mixing functions, using a single mixing function for both spin channels. Obtaining a common mixing function based on Eq. 38 is straightforward. Simply τ_σ needs to be replaced by $\tau_\sigma + \tau_{\sigma'}$, and $|\nabla\rho_{\sigma\sigma}|/\rho_\sigma$ is replaced by $|\nabla\rho_{\sigma\sigma} + 2\nabla\rho_{\sigma\sigma'} + \nabla\rho_{\sigma'\sigma'}|/(\rho_\sigma + \rho_{\sigma'})$ during the evaluation of $z^{\mathrm{DME}}_{\sigma\sigma'}$. For convenience, the MAPLE files of TMHF are part of the Supporting Information and can be included in the routines for LHFs.

The existing Kramers unrestricted two-component implementation [47] was reworked for efficiency and extended to include higher-order derivatives of the density, i.e. the Laplacian, Hessian, and the gradient of τ. This allows us to use the pig1, pig2, and tpig1 calibration function [18] as well as general metaGGAs for LHFs. Therefore, the LH20t functional [19] is now also available in two-component open-shell calculations. We further added interfaces to Libxc [87–89] to support (almost) all exchange and correlation functional ingredients. The revised thresholds of Ref. 30 are used for the numerical integration.[90,91] Note that the CF is neglected in the non-collinear two-component exchange-correlation kernel to avoid numerical instabilities.[30,54,55] The efficiency was increased by using the routines developed in Refs. 29 and 55, i.e. the screening procedure and memory handling described therein is applied in the general two-component case.

We note that the reworked LHF gradient routines evaluate the high-angular momentum contributions similar to the integral routines developed for the finite nucleus model in relativistic all-electron calculations.[92] Parallelization is available throughout with the OpenMP scheme.[93,94]

III. COMPUTATIONAL DETAILS

We will limit the assessment of accuracy to thermochemistry, excitation energies, and EPR properties in the main text. Further studies on magnetizabilities, polarizabilities, NMR spin-spin coupling constants, as well as NMR shielding constants and shifts are presented in the Supporting Information. The respective computational details are also given therein.

A. Thermochemistry

Atomization energies and barrier heights are important quality measures for DFAs. They yield a first overview of the general quality of a functionals, and are themselves commonly used when new, parameterized functionals are designed. Atomization energies were assessed for the W4-11 test set,[95] and barrier heights for the BH76 test set.[96–98] Both of those sets are subsets of the extensive "general main group thermochemistry, kinetics, and noncovalent interactions" set (GMTKN).[99] To yield values which can be directly compared to the GMTKN values, the def2-QZVP basis set [100] was used throughout, in conjunction with a large integration grid (grid 5) for numerical integration.[90,91] Results for other functionals are taken from Ref. 99. To provide a comprehensive overview, we compare to a variety of density functionals commonly used nowadays, as well as earlier designed local hybrid functionals that have been fitted to thermochemical data. This includes the metaGGAs TPSS,[9] Tao–Mo,[36] SCAN,[37] the hybrid functionals PBE0,[7,8] B3LYP,[4–6] TPSSh,[9,10] the range-separated functionals CAM-B3LYP,[14] LC-ωPBE,[101] ωB97X-D,[102] and the local hybrid functionals LH12ct-SsirPW92,[48] LH14t-calPBE,[17] and LH20t.[19]

B. Excitation Energies

For the excitation energies, we consider the benchmark test set of Suellen and co-workers with experimental reference results, which match third-order coupled cluster (CC3) values to within 0.05 eV or less.[103] Structures were taken from Ref. 103. In line with this reference, we use the aug-cc-pVTZ basis set [79–81] and large grids (grid size 4) for the numerical integration of the DFT parts.[90,91] Tight SCF thresholds of 10^{-9} Hartree for the energy and 10^{-7} a.u. for the root mean square of the density matrix are applied. Response equations are converged with a threshold of 10^{-5} a.u. for the norm of the residuum.[104] The excitation energies are corrected by the B3LYP zero-point vibrational energies.[105] Excitation energies have been evaluated using the functionals also used in the previous section. Results with conventional functionals are taken from Ref. 103, while results with all previously designed local hybrids are taken from Ref. 29.

C. EPR Calculations

EPR properties such as the hyperfine coupling (HFC) constant and the g-tensor are challenging properties for local hybrid functionals due to the high-density limit.[47] We have re-

cently benchmarked EPR properties in a self-consistent spin–orbit exact two-component (X2C) framework.[106,107] Herein, we extent these studies to local hybrid functionals, those general two-component implementation is described in the main text. To do so, we consider the 17 small transition-metal complexes of Ref. 108, namely $[MoNCl_4]^{2-}$, $[MoOF_4]^{-}$, $[MoOCl_4]^{-}$, $[MoOF_5]^{2-}$, $[MoOBr_5]^{2-}$, $[WOCl_4]^{-}$, $[WOF_5]^{2-}$, $[WOBr_5]^{2-}$, $[TcNF_4]^{-}$, $[TcNCl_4]^{-}$, $[TcNBr_4]^{-}$, $[ReNF_4]^{-}$, $[ReNCl_4]^{-}$, $[ReNBr_4]^{-}$, $[ReOBr_4]$, $[ReOF_5]^{-}$, and $[OsOF_5]$. We use the same computational parameters as in Refs. 106 and 107. In detail, the x2c-QZVPall-2c basis set [109] is applied for all elements. Large grids (grid 5a) are chosen for the numerical integration.[90,91,110] The conductor-like screening model (COSMO) is applied with the default parameters to compensate the negative charge.[111,112] We use the X2C Hamiltonian in the diagonal local approximation to the unitary transformation (DLU).[30,92,106,107,113–116] The restricted kinetic balance (RKB) condition [117] is employed for the HFC, whereas both RKB and the restricted magnetic balance (RMB) condition [118] are employed for the *g*-tensor. An SCF threshold of 10^{-9} Hartree is applied. In addition to the functionals used in the previous section and the Hartee–Fock method, we consider the following DFAs additionally to provide a more complete overview in this chapter, as data is yet comparably rare. S-VWN,[119–121] KT3,[122] BP86,[31,123] PBE,[7] revTPSS,[124,125] r^{2}SCAN,[38,39] BH&HLYP,[5,31,126] PBE0 including 40% of HF exchange (PBE0-40HF),[7,8,108] B97,[127] B97-2,[128] revTPSSh,[124,125] TPSS0,[10,129] r^{2}SCANh,[38,39,130] r^{2}SCAN0,[38,39,130] r^{2}SCAN50,[38,39,130] CAM-QPT-00,[131] CAM-QTP-02,[132] HSE06,[133–135] LH12ct-SsifPW92,[48] LH20t* (LH20t without calibration function),[19] LHJ14,[22] mPSTS-a1,[28,29] and mPSTS-noa2.[28,29] Note that SCAN has been replaced by r^{2}SCAN, as HFC constants and *g*-tensors are considerably more sensitive to the integration grid.

IV. ASSESSMENT OF ACCURACY FOR THERMOCHEMISTRY

To assess the basic properties of the newly constructed functionals, their thermochemical properties are investigated. The W4-11[95] and BH76 subset [96–98] from the GMTKN55 test set [99] were chosen, outlining the principal capabilities of a density functional approximation (DFA) for the calculation of atomization energies (W4-11) and barrier heights (BH76). The results are displayed in Figs. 2 and 3.

TMHF is a major step forwards for functionals that have been designed from first principles. With MAE/RMSD values of 2.78/4.60 kcal/mol for the W4-11 atomization energy subset, and

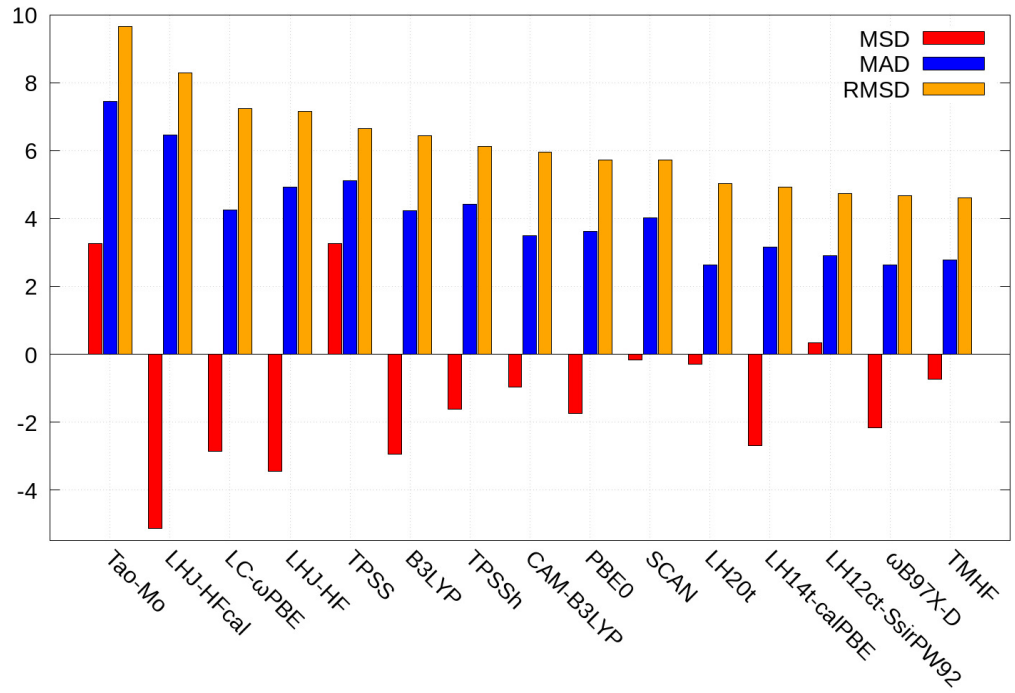

FIG. 2. Mean standard deviation (MSD), mean average deviation (MAD), and root mean square deviation (RMSD) for the atomization energies of the W4-11 test set. All values in kcal/mol.

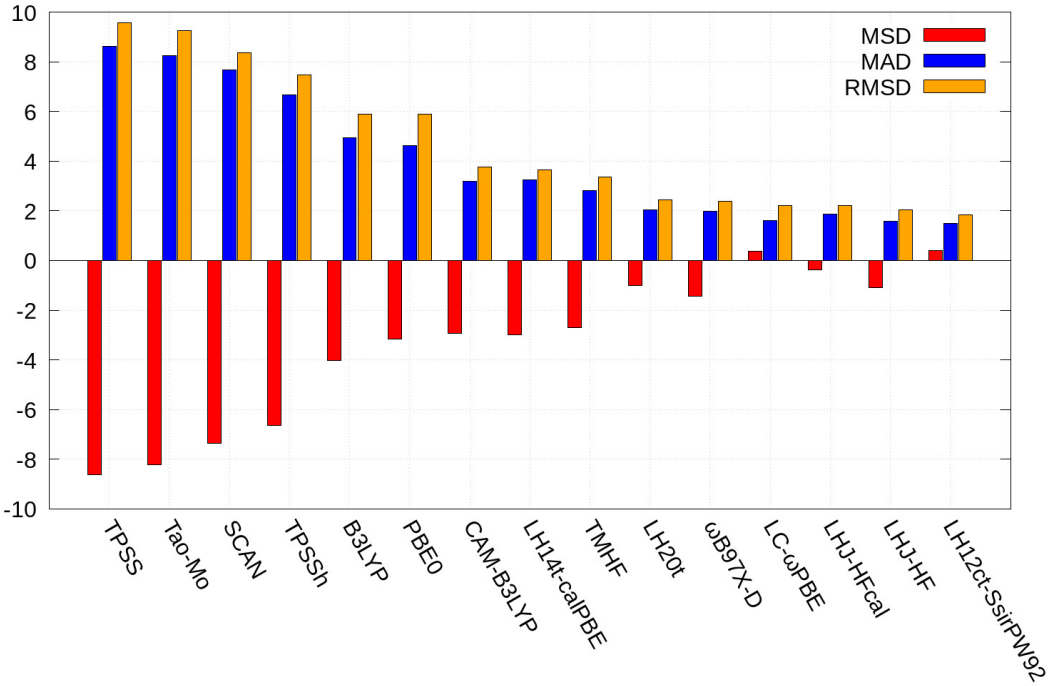

FIG. 3. Mean standard deviation (MSD), mean average deviation (MAD), and root mean square deviation (RMSD) for the barrier heights of the BH76 test set. All values in kcal/mol.

2.80/3.36 kcal/mol for the barrier heights of the BH76 subset, it outperforms any other functionals that has been constructed from first principles. Popular thermochemically optimized functionals such as ωB97X-D exhibit similar errors for the W4-11 subset. Furthermore, previously reported thermochemically optimized local hybrid functionals, as for example LH20t, are not able to significantly outperform TMHF. From a viewpoint of thermochemistry, therefore TMHF performs nearly as well as the best parameterized functionals. While for barrier heights parameterized functionals still hold an edge, the differences are rather small and probably do no longer outweigh the loss of generality.

Table III summarizes the errors of thermochemical properties for a set of DFAs that has been derived from first principles. Here, a clear trend is observed following Jacob's ladder. The most pronounced error reduction happens from GGA to metaGGAs, followed by the step to global hybrids. SCAN indeed is able to perform as well as global hybrids, still losing out for barrier heights. The latter are more sensitive to the inclusion of exact exchange, generally preferring functionals with a higher amount of exact exchange. The parameter-free local hybrid presented in this work, TMHF, again lowers the bar significantly. The statistical errors in barrier heights are nearly halved. Atomization energies are also improved by more than 1 kcal/mol on average, yet yielding a less pronounced underbinding when compared to the global hybrids TPSSh and PBE0.

TABLE III. Mean standard deviation (MSD), mean average deviation (MAD), and root mean square deviation (RMSD) for the atomization energies of the W4-11 test set and the barrier heights of the BH76 test set. All values in kcal/mol.

	W4-11			BH76		
	MSD	MAD	RMSD	MSD	MAD	RMSD
PBE	13.35	14.96	18.50	−9.11	9.15	10.39
Tao–Mo	3.27	7.45	9.66	−8.21	8.24	9.24
TPSS	3.27	5.11	6.65	−8.61	8.63	9.58
TPSSh	−1.62	4.41	6.12	−6.65	6.68	7.48
SCAN	−0.17	4.01	5.72	−7.36	7.66	8.37
PBE0	−1.75	3.62	5.73	−3.17	4.62	5.90
TMHF	−0.73	2.78	4.60	−2.71	2.80	3.36

V. ASSESSMENT OF ACCURACY FOR EXCITATION ENERGIES

The test set of Suellen *et al.*, which is composed of 41 excitation energies with accurate experimental and approximate coupled cluster singles, doubles, and triples (CC3) reference values has become a popular way of benchmarking the capabilities to predict excitation energies.[103] For these molecules, TMHF performs very well too as shown in Fig. 4.

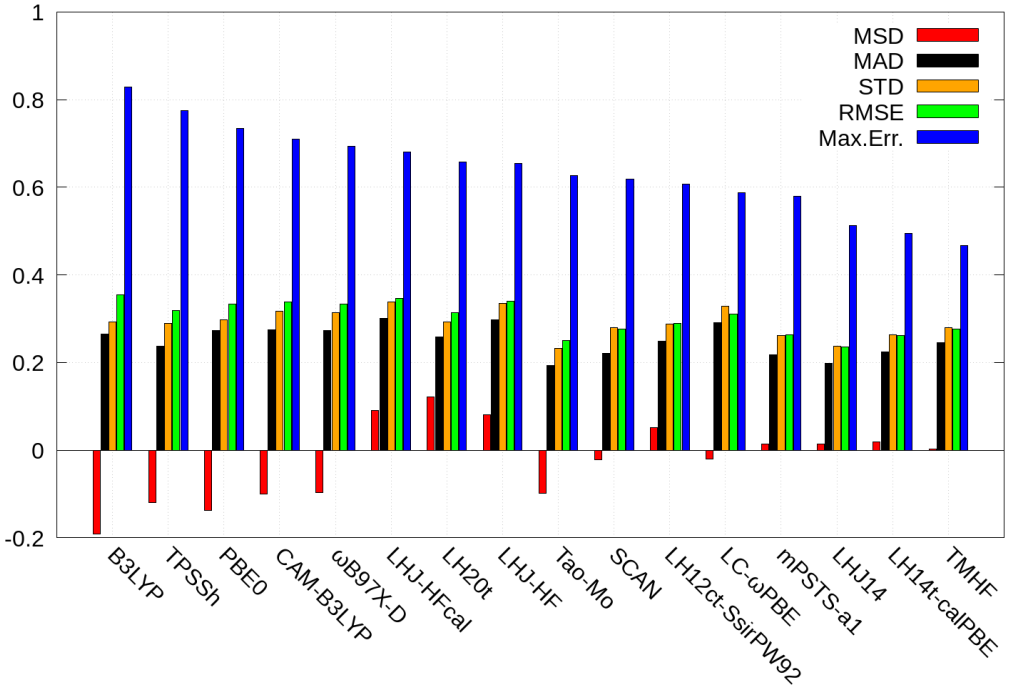

FIG. 4. Mean standard deviation (MSD), mean average deviation (MAD), standard deviation (STD), root mean square deviation (RMSD), and maximum error (Max.Err.) for 41 excitation energies of small molecules. All values in eV.

Most obviously, the parameterized functionals, which performed best for thermochemistry, are now no longer the top contenders. TMHF easily outperforms most other DFAs, though most statistical values are rather close for the top performers here. However, while overall performing very well, TMHF features the by far lowest maximum error of all functionals approximations that have been tested.[103] A maximum error of 0.46 eV equals a reduction of 0.1–0.3 eV compared to other popular DFAs. Even compared to coupled-cluster singles and doubles (CCSD), which exhibits a maximum error of 0.43 eV, it remains competitive. Common to most local hybrid functionals, the average deviation of TMHF is again centered around 0 eV. This outlines the balanced interpolation between local and exact exchange of the newly constructed TMHF local hybrid.

VI. ASSESSMENT OF ACCURACY FOR EPR PROPERTIES

The results for the HFC constant and the *g*-tensor are shown in Figs. 5 and 6, respectively. Here, the statistical evaluation of the *g*-tensor is shown with the RMB condition. The previous functional generation with LH12ct-SsirPW92 and LHJ14 does not yield accurate results. These functionals show larger errors than the conventional hybrid functionals. The mPSTS-noa2 and mPSTS-a1 functionals perform similar to established global hybrid functionals such as B3LYP, TPSSh, and the B97 family. However, it is outperformed by many range-separated hybrid functionals, TPSS0, and PBE0-40HF. Among the conventional hybrids, the latter show the smallest errors with MAPDs of 5–6% for the HFC constant and also yield smaller errors for the *g*-tensor (MAPDs of 13–18%).

TMHF performs remarkably well with an error of 4.77% for the HFC constant and 11.93% for the *g*-tensor. Thus, TMHF outperforms all other density functional approximations. This is also a remarkable improvement over the parent functional of Tao and Mo, which results in errors of 29.73% and 34.23%, respectively. The LH20t functional and the newly developed LHJ-HF functionals deliver similar results and are among the top performers with errors of about 7% for the HFC and 12–14% for the *g*-tensor. For LHJ-HF, the improvements can be mainly attributed to the re-optimized parameter for the admixture of HF exchange as EPR properties are sensitive towards the amount of exact exchange.[106,107]

The impact of the calibration function on the EPR properties is negligible, whereas it may lead to an unfavorable SCF convergence behavior due to the increased numerical difficulties of the higher order derivatives. This is especially important for two-component calculations, which require re-optimized thresholds for the numerical integration.[30,110] Thus, we recommend functionals without the calibration function for two-component calculations of open-shell compounds. The calibration function is also not used for the two-component exchange-correlation kernel of second-order properties to avoid numerical instabilities and inaccuracies.[29,30,54]

Taking together, local hybrid functionals are generally able to deliver accurate results for EPR parameters. Overall, TMHF outperforms all other functionals. The LH20t and LHJ-HF families lead to similar errors for the HFC constant and LHJ-HF shows minor improvements for the *g*-tensor. However, the functionals differ in the number of optimized parameters and the SCF convergence behavior, which deteriorates substantially with the CF. To illustrate the performance of local hybrid functionals for systems with more than one unpaired electron, we list the hyperfine coupling constants for $[TbPc_2]^-$ in the Supporting Information.

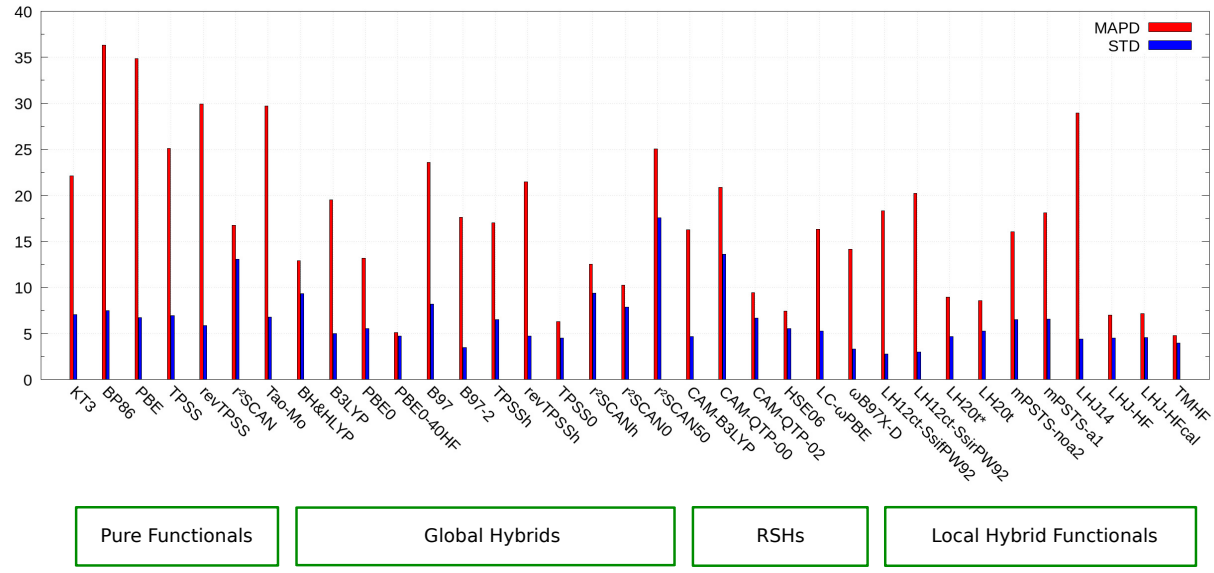

FIG. 5. Assessment of various density functional approximations for the HFC constant compared to the experimental findings for a set of 12 transition-metal complexes.[108] MAPD and STD denote the mean absolute percent-wise error and its standard deviation. The data of the conventional functionals are taken from Ref. 106.

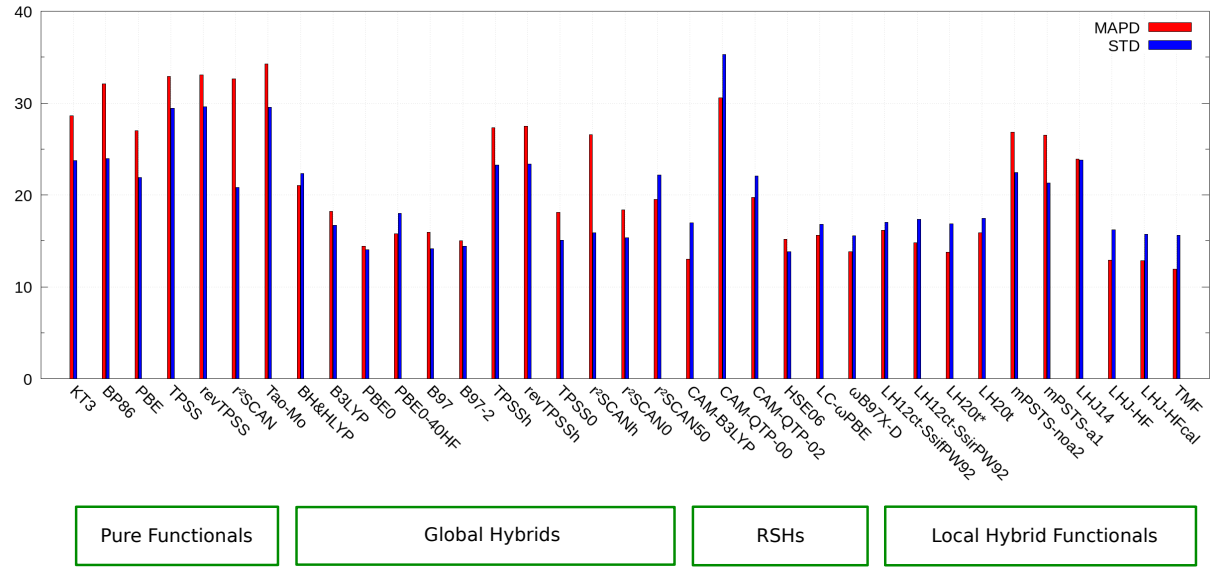

FIG. 6. Assessment of various density functional approximations for the Δg-shift compared to the experimental findings for the set of 17 transition-metal complexes.[108] MAPD and STD denote the mean absolute percent-wise error and its standard deviation. The data of the conventional functionals are taken from Ref. 107. $[TcNCl_4]^-$ and $[ReNBr_4]^-$ are neglected in the statistical evaluation.

VII. SUMMARY AND CONCLUSIONS

We derived a new local hybrid exchange approximation, termed TMHF, from first principles. For its construction, we only take into account the exact solution of the hydrogen atom, as well as the low-density and high-density limits of the exchange energies of two-electron systems. The derived functional is therefore not fitted to any bound systems or reaction energies. Statistical errors of thermochemical properties reveal that indeed the TMHF exchange model is a significant step forward for density functional approximations designed from first principles. Being the next step on rung 4 of Jacob's ladder,[136] TMHF significantly outperforms all previously presented approximations from first principles.

In subsequent investigations of various properties, the assumption that density functional approximation from first principles are generally applicable could be verified. For various properties such as the calculation of excited states, EPR parameters, or NMR coupling constants, TMHF is best in class. Not only does it provide significantly lower statistical errors, but also far lower maximum errors as compared to other leading functionals. This leads to more reliable predictions across different molecules and properties, which may have very different needs. There are, of course, still points where future work is desperately needed. For example, rather a simple local correlation model is used, not being able to truly describe multi-configurational settings. Furthermore, core-related properties such as NMR shifts are not improved, given the lack of exact exchange near the nucleus from our model. Finally, van–der–Waals interactions still need to be included using a dispersion correction model, as long range correlation can also not be modeled by our approach alone.

Despite the remaining deficiencies, we conclude that certainly TMHF is strikingly close to a one-for-all functional for the time being.

SUPPLEMENTARY MATERIAL

Supporting Information is available

- Individual results and statistical evaluation for magnetizabilities and polarizabilities
- Individual results and statistical evaluation for NMR spin–spin coupling constants
- Individual results and statistical evaluation for NMR shieldings and shifts
- Individual results for thermochemistry
- Individual results and statistical evaluation for excitation energies
- Individual results and statistical evaluation for hyperfine coupling constants and g-tensors
- Application to the isotropic EPR hyperfine coupling constant of $[TbPc_2]^-$
- Maple files of TMHF to allow for an easy incorporation into quantum chemical programs

AUTHOR'S CONTRIBUTIONS

C. Holzer and Y. J. Franzke contributed equally to this work.

ACKNOWLEDGMENTS

C.H. gratefully acknowledges funding by the Volkswagen Foundation. Y.J.F. acknowledges financial support by TURBOMOLE GmbH.

DATA AVAILABILITY STATEMENT

The data that support the findings of this study are available within the article and its supplementary material.

REFERENCES

[1]G. I. Csonka, J. P. Perdew, and A. Ruzsinszky, J. Chem. Theory Comput. **6**, 3688 (2010).

[2]A. D. Becke, J. Chem. Phys. **140**, 18A301 (2014).

[3]N. Mardirossian and M. Head-Gordon, Mol. Phys. **115**, 2315 (2017).

[4]A. D. Becke, J. Chem. Phys. **98**, 5648 (1993).

[5]C. Lee, W. Yang, and R. G. Parr, Phys. Rev. B **37**, 785 (1988).

[6]P. J. Stephens, F. J. Devlin, C. F. Chabalowski, and M. J. Frisch, J. Phys. Chem. **98**, 11623 (1994).

[7]J. P. Perdew, K. Burke, and M. Ernzerhof, Phys. Rev. Lett. **77**, 3865 (1996).

[8]C. Adamo and V. Barone, J. Chem. Phys. **110**, 6158 (1999).

[9]J. Tao, J. P. Perdew, V. N. Staroverov, and G. E. Scuseria, Phys. Rev. Lett. **91**, 146401 (2003).

[10]V. N. Staroverov, G. E. Scuseria, J. Tao, and J. P. Perdew, J. Chem. Phys. **119**, 12129 (2003).

[11]P. W. Gill, R. D. Adamson, and J. A. Pople, Mol. Phys. **88**, 1005 (1996).

[12]T. Leininger, H. Stoll, H.-J. Werner, and A. Savin, Chem. Phys. Lett. **275**, 151 (1997).

[13]Y. Tawada, T. Tsuneda, S. Yanagisawa, T. Yanai, and K. Hirao, J. Chem. Phys. **120**, 8425 (2004).

[14]T. Yanai, D. P. Tew, and N. C. Handy, Chem. Phys. Lett. **393**, 51 (2004).

[15]J. Jaramillo, G. E. Scuseria, and M. Ernzerhof, J. Chem. Phys. **118**, 1068 (2003).

[16]J. Tao, V. N. Staroverov, G. E. Scuseria, and J. P. Perdew, Phys. Rev. A **77**, 012509 (2008).

[17]A. V. Arbuznikov and M. Kaupp, J. Chem. Phys. **141**, 204101 (2014).

[18]T. M. Maier, M. Haasler, A. V. Arbuznikov, and M. Kaupp, Phys. Chem. Chem. Phys. **18**, 21133 (2016).

[19]M. Haasler, T. M. Maier, R. Grotjahn, S. Gückel, A. V. Arbuznikov, and M. Kaupp, J. Chem. Theory Comput. **16**, 5645 (2020).

[20]T. M. Henderson, B. G. Janesko, and G. E. Scuseria, J. Phys. Chem. A **112**, 12530 (2008).

[21]T. M. Maier, A. V. Arbuznikov, and M. Kaupp, Wiley Interdiscip. Rev.: Comput. Mol. Sci. **9**, e1378 (2018).

[22]E. R. Johnson, J. Chem. Phys. **141**, 124120 (2014).

[23]A. V. Arbuznikov and M. Kaupp, Chem. Phys. Lett. **440**, 160 (2007).

[24]T. Schmidt, E. Kraisler, A. Makmal, L. Kronik, and S. Kümmel, J. Chem. Phys. **140**, 18A510 (2014).

[25]P. de Silva and C. Corminboeuf, J. Chem. Theory Comput. **10**, 3745 (2014).

[26]P. de Silva and C. Corminboeuf, J. Chem. Phys. **142**, 074112 (2015).

[27]A. Görling and M. Levy, Phys. Rev. A **50**, 196 (1994).

[28]J. P. Perdew, V. N. Staroverov, J. Tao, and G. E. Scuseria, Phys. Rev. A **78**, 052513 (2008).

[29]C. Holzer, Y. J. Franzke, and M. Kehry, J. Chem. Theory Comput. **17**, 2928 (2021).

[30]Y. J. Franzke, F. Mack, and F. Weigend, J. Chem. Theory Comput. **17**, 3974 (2021).

[31]A. D. Becke, Phys. Rev. A **38**, 3098 (1988).

[32]A. D. Becke, J. Chem. Phys. **88**, 1053 (1988).

[33]A. D. Becke, J. Chem. Phys. **104**, 1040 (1996).

[34]M. G. Medvedev, I. S. Bushmarinov, J. Sun, J. P. Perdew, and K. A. Lyssenko, Science **355**, 49 (2017).

[35]A. D. Becke, J. Chem. Phys. (2022), 10.1063/5.0091198.

[36]J. Tao and Y. Mo, Phys. Rev. Lett. **117**, 073001 (2016).

[37]J. Sun, A. Ruzsinszky, and J. P. Perdew, Phys. Rev. Lett. **115**, 036402 (2015).

[38]J. W. Furness, A. D. Kaplan, J. Ning, J. P. Perdew, and J. Sun, J. Phys. Chem. Lett. **11**, 8208 (2020).

[39]J. W. Furness, A. D. Kaplan, J. Ning, J. P. Perdew, and J. Sun, J. Phys. Chem. Lett. **11**, 9248 (2020).

[40]M. Dolg and X. Cao, Chem. Rev. **112**, 403 (2012).

[41]J. Autschbach, J. Chem. Phys. **136**, 150902 (2012).

[42]T. Saue, ChemPhysChem **12**, 3077 (2011).

[43]P. Pyykkö, Annu. Rev. Phys. Chem. **63**, 45 (2012).

[44]K. G. Dyall and K. Fægri Jr., *Introduction to Relativistic Quantum Chemistry* (Oxford University Press, New York, USA, 2007).

[45]M. Reiher and A. Wolf., *Relativistic Quantum Chemistry – The Fundamental Theory of Molecular Science*, 2nd ed. (Wiley-VCH, Weinheim, Germany, 2015).

[46]W. Liu, ed., *Handbook of Relativistic Quantum Chemistry* (Springer, Berlin, Heidelberg, 2017).

[47]A. Wodyński and M. Kaupp, J. Chem. Theory Comput. **16**, 314 (2020).

[48]A. V. Arbuznikov and M. Kaupp, J. Chem. Phys. **136**, 014111 (2012).

[49]P. Plessow and F. Weigend, J. Comput. Chem. **33**, 810 (2012).

[50]H. Bahmann and M. Kaupp, J. Chem. Theory Comput. **11**, 1540 (2015).

[51]S. Klawohn, H. Bahmann, and M. Kaupp, J. Chem. Theory Comput. **12**, 4254 (2016).

[52]T. M. Maier, H. Bahmann, and M. Kaupp, J. Chem. Theory Comput. **11**, 4226 (2015).

[53]R. Grotjahn, F. Furche, and M. Kaupp, J. Chem. Theory Comput. **15**, 5508 (2019).

[54]M. Kehry, Y. J. Franzke, C. Holzer, and W. Klopper, Mol. Phys. **118**, e1755064 (2020).

[55]C. Holzer, J. Chem. Phys. **153**, 184115 (2020).

[56]Y. J. Franzke, C. Holzer, and F. Mack, . Chem. Theory Comput. **18**, 1030 (2022).

[57]C. J. Schattenberg, K. Reiter, F. Weigend, and M. Kaupp, J. Chem. Theory Comput. **16**, 931 (2020).

[58]F. Mack, C. J. Schattenberg, M. Kaupp, and F. Weigend, J. Phys. Chem. A **124**, 8529 (2020).

[59]C. J. Schattenberg and M. Kaupp, J. Chem. Theory Comput. **17**, 1469 (2021).

[60]C. J. Schattenberg and M. Kaupp, J. Phys. Chem. A **125**, 2697 (2021).

[61]C. F. von Weizsäcker, Z. Phys. **96**, 431 (1935).

[62]F. G. Cruz, K.-C. Lam, and K. Burke, J. Phys. Chem. A **102**, 4911 (1998).

[63]K. Burke, F. G. Cruz, and K.-C. Lam, J. Chem. Phys. **109**, 8161 (1998).

[64]A. D. Becke, J. Chem. Phys. **109**, 2092 (1998).

[65]C. Van Wüllen, J. Comput. Chem. **20**, 51 (1999).

[66]C. Van Wüllen, J. Comput. Chem. **23**, 779 (2002).

[67]M. K. Armbruster, F. Weigend, C. van Wüllen, and W. Klopper, Phys. Chem. Chem. Phys. **10**, 1748 (2008).

[68]J. Autschbach, Mol. Phys. **111**, 2544 (2013).

[69]A. Baldes and F. Weigend, Mol. Phys. **111**, 2617 (2013).

[70]H. Bahmann, A. Rodenberg, A. V. Arbuznikov, and M. Kaupp, J. Chem. Phys. **126**, 011103 (2007).

[71]A. Pausch and C. Holzer, J. Chem. Phys. Lett. **13**, 4335 (2022).

[72]Y. Mo, R. Car, V. N. Staroverov, G. E. Scuseria, and J. Tao, Phys. Rev. B **95**, 035118 (2017).

[73]S. Jana, A. Patra, and P. Samal, J. Chem. Phys. **149**, 044120 (2018).

[74]A. Patra, S. Jana, and P. Samal, J. Phys. Chem. A **123**, 10582 (2019).

[75]C. J. Umrigar and X. Gonze, Phys. Rev. A **50**, 3827 (1994).

[76]J. P. Perdew, A. Ruzsinszky, J. Sun, and K. Burke, J. Chem. Phys. **140**, 18A533 (2014).

[77]T. Aschebrock and S. Kümmel, Phys. Rev. Res. **1**, 033082 (2019).

[78]J. W. Furness, N. Sengupta, J. Ning, A. Ruzsinszky, and J. Sun, J. Chem. Phys. **152**, 244112 (2020).

[79]T. H. Dunning, J. Chem. Phys. **90**, 1007 (1989).

[80]R. A. Kendall, T. H. Dunning, and R. J. Harrison, J. Chem. Phys. **96**, 6796 (1992).

[81]D. E. Woon and T. H. Dunning, J. Chem. Phys. **98**, 1358 (1993).

[82]Developers' version of TURBOMOLE V7.6 2021, a development of University of Karlsruhe and Forschungszentrum Karlsruhe GmbH, 1989-2007, TURBOMOLE GmbH, since 2007; available from `https://www.turbomole.org` (retrieved January 12, 2022).

[83]R. Ahlrichs, M. Bär, M. Häser, H. Horn, and C. Kölmel, Chem. Phys. Lett. **162**, 165 (1989).

[84]F. Furche, R. Ahlrichs, C. Hättig, W. Klopper, M. Sierka, and F. Weigend, Wiley Interdiscip. Rev.: Comput. Mol. Sci. **4**, 91 (2014).

[85]S. G. Balasubramani, G. P. Chen, S. Coriani, M. Diedenhofen, M. S. Frank, Y. J. Franzke, F. Furche, R. Grotjahn, M. E. Harding, C. Hättig, A. Hellweg, B. Helmich-Paris, C. Holzer, U. Huniar, M. Kaupp, A. Marefat Khah, S. Karbalaei Khani, T. Müller, F. Mack, B. D. Nguyen, S. M. Parker, E. Perlt, D. Rappoport, K. Reiter, S. Roy, M. Rückert, G. Schmitz, M. Sierka, E. Tapavicza, D. P. Tew, C. van Wüllen, V. K. Voora, F. Weigend, A. Wodyński, and J. M. Yu, J. Chem. Phys. **152**, 184107 (2020).

[86]"MAPLE," Version 2020, available from `https://www.maplesoft.com/` (retrieved December 6, 2020).

[87]"Libxc," 5.1.7, available from `https://www.tddft.org/programs/libxc/` (retrieved July 30, 2021).

[88]M. A. L. Marques, M. J. T. Oliveira, and T. Burnus, Comput. Phys. Commun. **183**, 2272 (2012).

[89]S. Lehtola, C. Steigemann, M. J. T. Oliveira, and M. A. L. Marques, SoftwareX **7**, 1 (2018).

[90]O. Treutler and R. Ahlrichs, J. Chem. Phys. **102**, 346 (1995).

[91]O. Treutler, *Entwicklung und Anwendung von Dichtefunktionalmethoden*, Dissertation (Dr. rer. nat.), University of Karlsruhe (TH), Germany (1995).

[92]Y. J. Franzke, N. Middendorf, and F. Weigend, J. Chem. Phys. **148**, 104410 (2018).

[93]OpenMP Architecture Review Boards, "OpenMP API shared-memory parallel programming," `https://www.openmp.org` (retrieved September 26, 2021).

[94]C. Holzer and Y. J. Franzke, OpenMP version of ridft, rdgrad, and egrad with contributions to mpshift, dscf, and grad; improved OpenMP version of aoforce and escf, released with TURBOMOLE V7.4 and further improved in TURBOMOLE V7.5.

[95]A. Karton, S. Daon, and J. M. Martin, Chem. Phys. Lett. **510**, 165 (2011).

[96]Y. Zhao, N. González-García, and D. G. Truhlar, J. Phys. Chem. A **109**, 2012 (2005).

[97]Y. Zhao, B. J. Lynch, and D. G. Truhlar, Phys. Chem. Chem. Phys. **7**, 43 (2005).

[98]L. Goerigk and S. Grimme, J. Chem. Theory Comput. **6**, 107 (2010).

[99]L. Goerigk, A. Hansen, C. Bauer, S. Ehrlich, A. Najibi, and S. Grimme, Phys. Chem. Chem. Phys. **19**, 32184 (2017).

[100]F. Weigend and R. Ahlrichs, Phys. Chem. Chem. Phys. **7**, 3297 (2005).

[101]O. A. Vydrov and G. E. Scuseria, J. Chem. Phys. **125**, 234109 (2006).

[102]J.-D. Chai and M. Head-Gordon, Phys. Chem. Chem. Phys. **10**, 6615 (2008).

[103]C. Suellen, R. G. Freitas, P.-F. Loos, and D. Jacquemin, J. Chem. Theory Comput. **15**, 4581 (2019).

[104]F. Furche, B. T. Krull, B. D. Nguyen, and J. Kwon, J. Chem. Phys. **144**, 174105 (2016).

[105]P.-F. Loos and D. Jacquemin, J. Chem. Theory Comput. **15**, 2481 (2019).

[106]Y. J. Franzke and J. M. Yu, J. Chem. Theory Comput. **18**, 323 (2022).

[107]Y. J. Franzke and J. M. Yu, J. Chem. Theory Comput. **18**, 2246 (2022).

[108]S. Gohr, P. Hrobárik, M. Repiský, S. Komorovský, K. Ruud, and M. Kaupp, J. Phys. Chem. A **119**, 12892 (2015).

[109]Y. J. Franzke, L. Spiske, P. Pollak, and F. Weigend, J. Chem. Theory Comput. **16**, 5658 (2020).

[110]Y. J. Franzke, R. Treß, T. M. Pazdera, and F. Weigend, Phys. Chem. Chem. Phys. **21**, 16658 (2019).

[111]A. Klamt and G. Schüürmann, J. Chem. Soc., Perkin Trans. 2 , 799 (1993).

[112]A. Schäfer, A. Klamt, D. Sattel, J. C. W. Lohrenz, and F. Eckert, Phys. Chem. Chem. Phys. **2**, 2187 (2000).

[113]D. Peng and M. Reiher, J. Chem. Phys. **136**, 244108 (2012).

[114]D. Peng, N. Middendorf, F. Weigend, and M. Reiher, J. Chem. Phys. **138**, 184105 (2013).

[115]Y. J. Franzke and F. Weigend, J. Chem. Theory Comput. **15**, 1028 (2019).

[116]S. Gillhuber, Y. J. Franzke, and F. Weigend, J. Phys. Chem. A **125**, 9707 (2021).

[117]R. E. Stanton and S. Havriliak, J. Chem. Phys. **81**, 1910 (1984).

[118]S. Komorovský, M. Repiský, O. L. Malkina, V. G. Malkin, I. Malkin Ondík, and M. Kaupp, J. Chem. Phys. **128**, 104101 (2008).

[119]P. A. M. Dirac, Proc. Roy. Soc. Lond. A **123**, 714 (1929).

[120]J. C. Slater, Phys. Rev. **81**, 385 (1951).

[121]S. H. Vosko, L. Wilk, and M. Nusair, Can. J. Phys. **58**, 1200 (1980).

[122]T. W. Keal and D. J. Tozer, J. Chem. Phys. **121**, 5654 (2004).

[123]J. P. Perdew, Phys. Rev. B **33**, 8822 (1986).

[124]J. P. Perdew, A. Ruzsinszky, G. I. Csonka, L. A. Constantin, and J. Sun, Phys. Rev. Lett. **103**, 026403 (2009).

[125]J. P. Perdew, A. Ruzsinszky, G. I. Csonka, L. A. Constantin, and J. Sun, Phys. Rev. Lett. **106**, 179902 (2011).

[126]A. D. Becke, J. Chem. Phys. **98**, 1372 (1993).

[127]A. D. Becke, J. Phys. Chem. **107**, 8554 (1997).

[128]P. J. Wilson, T. J. Bradley, and D. J. Tozer, J. Chem. Phys. **115**, 9233 (2001).

[129]S. Grimme, J. Phys. Chem. A **109**, 3067 (2005).

[130]M. Bursch, H. Neugebauer, S. Ehlert, and S. Grimme, J. Chem. Phys. **156**, 134105 (2022).

[131]Y. Jin and R. J. Bartlett, J. Chem. Phys. **145**, 034107 (2016).

[132]R. L. A. Haiduke and R. J. Bartlett, J. Chem. Phys. **149**, 131101 (2018).

[133]J. Heyd, G. E. Scuseria, and M. Ernzerhof, J. Chem. Phys. **118**, 8207 (2003).

[134]J. Heyd, G. E. Scuseria, and M. Ernzerhof, J. Phys. Chem. **124**, 219906 (2006).

[135]A. V. Krukau, O. A. Vydrov, A. F. Izmaylov, and G. E. Scuseria, J. Phys. Chem. **125**, 224106 (2006).

[136]J. P. Perdew and K. Schmidt, AIP Conf. Proc. **577**, 1 (2001).